

DOT/FAA/AR-11/1,P1

Federal Aviation Administration
William J. Hughes Technical Center
Aviation Research Division
Atlantic City International Airport
New Jersey 08405

Adhesively Bonded Joints

Part 1: Bondline Thickness Effects and Hybrid Design of Adhesively Bonded Joints

February 2014

Final Report

This document is available to the U.S. public through the National Technical Information Services (NTIS), Springfield, Virginia 22161.

This document is also available from the Federal Aviation Administration William J. Hughes Technical Center at actlibrary.tc.faa.gov.



U.S. Department of Transportation
Federal Aviation Administration

NOTICE

This document is disseminated under the sponsorship of the U.S. Department of Transportation in the interest of information exchange. The U.S. Government assumes no liability for the contents or use thereof. The U.S. Government does not endorse products or manufacturers. Trade or manufacturers' names appear herein solely because they are considered essential to the objective of this report. The findings and conclusions in this report are those of the author(s) and do not necessarily represent the views of the funding agency. This document does not constitute FAA policy. Consult the FAA sponsoring organization listed on the Technical Documentation page as to its use.

This report is available at the Federal Aviation Administration William J. Hughes Technical Center's Full-Text Technical Reports page: actlibrary.tc.faa.gov in Adobe Acrobat portable document format (PDF).

1. Report No. DOT/FAA/AR-11/1,P1		2. Government Accession No.		3. Recipient's Catalog No.	
4. Title and Subtitle ADHESIVELY BONDED JOINTS, PART 1: BONDLINE THICKNESS EFFECTS AND HYBRID DESIGN OF ADHESIVELY BONDED JOINTS		5. Report Date February 2014		6. Performing Organization Code	
		7. Author(s) CT Sun		8. Performing Organization Report No.	
9. Performing Organization Name and Address Purdue University 155 S. Grant Street West Lafayette, IN 47907-2114		10. Work Unit No. (TRAIS)		11. Contract or Grant No.	
		12. Sponsoring Agency Name and Address U.S. Department of Transportation Federal Aviation Administration Aviation Safety—Aircraft Certification Service—Aircraft Engineering Division 1601 Lind Ave., SW Renton, WA 98057		13. Type of Report and Period Covered Final Report 2004-2010	
				14. Sponsoring Agency Code AIR-100	
15. Supplementary Notes The Federal Aviation Administration William J. Hughes Technical Center Aviation Research Division Technical Monitor was Lynn Pham.					
16. Abstract <p>This report details work conducted at Purdue University under the Federal Aviation Administration (FAA) Joint Advanced Materials and Structures Center of Excellence (JAMS-COE) program advancing knowledge on adhesively bonded structures, and addresses the issues of the correlation between bondline thickness and fracture, as well as the design of hybrid adhesively bonded joints. This report is one of three reports generated by the FAA JAMS-COE program.</p> <p>In this work, the characterization of fracture toughness in mode I loading under the consideration of bondline thickness effect was investigated. Double cantilever beams were tested to obtain fracture data for bonded joints with varying adhesive thickness. The concept of the critical crack tip opening angle (CTOA) was investigated both analytically and experimentally. The value of the CTOA is not influenced appreciably by the adhesive thickness when the failure mode remains mode I, failure of the adhesive. Consequently, the adhesive thickness effect on the strength of the joint can be accounted for by a constant CTOA. However, if the failure for very small adhesive thicknesses is shifted to the interface between aluminum and the adhesive, the CTOA is no longer constant at failure.</p> <p>New designs for the bonded/bolted hybrid joints were investigated. The new designs incorporated additional composite straps that were bonded to the adherends. It was demonstrated by test and analysis that such a novel design would lead to more efficient joints. Finite element analysis results indicate that the hybrid joint with stepped attachments have the lowest peel stresses of all joints investigated.</p>					
17. Key Words Fracture mechanics, Local failure criterion, Adhesive bonding, Hybrid joint design, Adhesive thickness, Crack tip opening angle			18. Distribution Statement This document is available to the U.S. public through the National Technical Information Service (NTIS), Springfield, Virginia 22161. This document is also available from the Federal Aviation Administration William J. Hughes Technical Center at actlibrary.tc.faa.gov .		
19. Security Classif. (of this report) Unclassified		20. Security Classif. (of this page) Unclassified		21. No. of Pages 36	22. Price

TABLE OF CONTENTS

	Page
EXECUTIVE SUMMARY	vii
1. EFFECT OF BONDLINE THICKNESS ON FRACTURE TOUGHNESS IN ADHESIVELY BONDED JOINTS	1
1.1 Introduction	1
1.2 Fracture Experiment	3
1.3 The K-Field Representation	5
1.4 The CTOA as a Fracture Parameter	8
1.5 Interfacial Failure	10
1.6 Crack Tip Opening Angle—Criterion and Analysis	13
2. DEVELOPMENT OF FAIL-SAFE HYBRID JOINTS	15
2.1 Introduction	15
2.2 Experiments	17
2.3 Results and Discussion	19
2.3.1 Bonded and Bolted Joint	19
2.3.2 Conventional Hybrid Joint	20
2.3.3 New Hybrid Joint With Attachments	21
2.3.4 Comparison of All Joint Configurations	22
2.3.5 Finite Element Analysis	23
2.3.6 Peel Stress Distribution	24
2.3.7 Load Distribution	25
3. CONCLUSIONS	26
3.1 Effects of Bondline Thickness Conclusions	26
3.2 Hybrid Joint Design Conclusions	26
4. REFERENCES	26

LIST OF FIGURES

Figure		Page
1	Adhesive Thickness Effect on Strength for Mode I Fracture	2
2	Traditional Explanation of Thickness Effect on Strength of Joints	2
3	Specimen Configuration	3
4	Load vs. Displacement Curves for Specimens With Different Adhesive Layer Thicknesses: Thicker Specimens, Stable Load Decreases After Peak Load and Thinner Specimens, Sudden Load Drop After Peak Load	4
5	Experimental Results of Specimen Strength vs. Bondline Thickness	4
6	Configuration of the Finite Element Model	5
7	Typical FEA Mesh of DCB Specimens	5
8	Energy Release Rate of DCB Specimens With Various Bondline Thicknesses	5
9	Degree of Singularity for DCB Specimens With Different Bondline Thicknesses	6
10	Stress-Strain Curve of Hysol EA 9394 Adhesive Material	7
11	DCB Models' Plastic Zone Sizes Under Failure Load: DCB Model With 0.4-mm Adhesive Thickness and DCB Model With 0.8-mm Adhesive Thickness	8
12	The Angle Change Before Crack Initiation: Initial State and Loaded	9
13	Calculation of CTOA	9
14	Crack Tip Opening Angle vs. Adhesive Thickness	9
15	Crack Propagation for Specimens With Different Adhesive Layer Thicknesses (a) in Thicker Specimens, the Crack Initiated and Propagated Within the Adhesive Layer and (b) in Thinner Specimens, Interface Failure Occurred Before Crack Propagation	10
16	Maximum Stress Components Along the Interface vs. Load (Location and Value): Maximum Normal Stress and Maximum Shear Stress	11
17	Normal Stress Distribution Along Interface Near Crack Tip	12
18	Natural Initial Crack Configuration and Crack Tip Created by the Razorblade	13
19	The CTOA Values at a Constant Applied Load From Models With Different Initial Crack Configurations	14

20	The CTOA Values Under Thickness-Dependent Failure Load	14
21	Mode I Fracture Strength Prediction Using the Constant CTOA Criterion	15
22	Conventional Hybrid (Bonded/Bolted) Joint	16
23	Hybrid Joint With Angular Attachments	17
24	New Hybrid Joint With L-Shaped Attachments	17
25	Final Joint Configurations	18
26	Magnified View of the L-Shaped and Stepped Attachments	18
27	Load-Displacement Curve for the Composite Bonded Joint	19
28	Load-Displacement Curve for the Composite Bolted Joint	19
29	A Typical Shear-Out Failure Pattern Around the Bolt	20
30	Load-Displacement Curve for the Conventional Hybrid Joint	21
31	Load-Displacement Curves for Hybrid Joint With Attachments	22
32	Load-Displacement Curves for All Joints	23
33	Comparison of Failure Loads for All Joint Configurations	23
34	A Typical Stress Pattern for Three Joint Configurations	24
35	Peel Stress Distribution Along the Main Interface	24
36	Peel Stress Distribution Along the Interface of the Attachment and the Adherend	25
37	Load Distribution in the Hybrid Joint With L-Shaped Attachment	25

LIST OF ACRONYMS

CTOA	Crack tip opening angle
DCB	Double cantilever beam
FAA	Federal Aviation Administration
FEA	Finite element analysis
JAMS-COE	Joint Advanced Materials and Structures Center of Excellence
LEFM	Linear elastic fracture mechanics

EXECUTIVE SUMMARY

This report details work conducted at Purdue University under the Federal Aviation Administration (FAA) Joint Advanced Materials and Structures Center of Excellence (JAMS-COE) program advancing knowledge on adhesively bonded structures, and addresses the issues of the correlation between bondline thickness and fracture, as well as the design of hybrid adhesive joints. This report is one of three reports generated by the FAA JAMS-COE program.

In this report, the bondline thickness effect was investigated by experiment and analysis by characterization of mode I fracture toughness. Double cantilever beams (DCB), consisting of aluminum adherends and Hysol[®] EA 9394[™] adhesive with different thicknesses of the adhesive, were tested to obtain fracture data. The critical energy release rates of the DCB specimens were calculated by a crack closure method. It was found that the DCB specimen was not suitable for testing mode I fracture toughness of adhesive materials because of the exceedingly small K dominance zone sizes it can produce. An elastic-plastic analysis is needed to predict the failure of the DCB specimens. The DCB data and analysis were also used to investigate the concept of the critical crack tip opening angle (CTOA). The value of the CTOA is not influenced appreciably by the adhesive thickness when the failure mode remains mode I, failure of the adhesive. Consequently, the adhesive thickness effect on the strength of the joint can be accounted for by a constant CTOA. However, if the failure, for very small adhesive thicknesses, is shifted to the interface between aluminum and the adhesive the CTOA is no longer constant at failure.

New designs for the bonded/bolted hybrid joints were investigated where the bolt contributed to load transfer as soon as the joint was loaded. The new designs of composite bonded/bolted joints incorporated additional shapes that were bonded to the adherends. It was demonstrated by test and analysis that such a novel design resulted in more efficient joints. Finite element analysis results indicate that the hybrid joint with stepped attachments have the lowest peel stresses of all joints investigated.

1. EFFECT OF BONDLINE THICKNESS ON FRACTURE TOUGHNESS IN ADHESIVELY BONDED JOINTS.

1.1 INTRODUCTION.

Composites have been joined using mechanical fasteners or structural adhesives in various structural applications. Because aircraft structures are, in general, an assembly of many small or large parts, joining parts is an important technology. In metallic structural joints, mechanical fastening has been the most commonly used jointing technique. For composite joints, fiber breakage and stress concentration around the bolt location are avoided if adhesive bonding is used. There are other advantages in using adhesive bonding in composite structural joints, including lower weight penalty. Controlling the quality of bonded joints as well as predicting their strength is difficult, if not impossible. Therefore, a fail-safe design approach is commonly adopted where mechanical fasteners are used in addition to the adhesive bond. The combination of bonded and mechanical fastening is usually called a hybrid joint or bolted/bonded joint.

Significant amounts of composite materials are used in new commercial jetliners, such as the Boeing 787 and Airbus 350, as well as in small and mid-sized aircraft. Many composite-to-composite and composite-to-metal components are bonded by adhesives, in both primary and secondary load-bearing structures. It is well known that failure prediction remains a difficult problem in composites and in adhesively bonded joints. For adhesively bonded, built-up structures, failure is even more difficult to predict due to the complexities of geometric details and loading. Being able to definitively predict failure is a necessary technology that needs further research for reasons related to safety, performance, and cost. Flaws and damage, such as matrix cracks and delamination within the composite and debonding within joints, are difficult to detect and can potentially lead to catastrophic failure. Such damage forms, when detected, also present significant challenges within the context of repair. Efficient repairs to cracked metal and composite structures are achieved by adhesively bonding a composite patch over the damaged zone. An additional component of complexity arises when considering the durability of bonded composite structures: degradation of polymers (composite matrix and adhesive) can occur due to long-term environmental exposure, thereby negatively impacting the fracture and fatigue characteristics of these materials.

Adhesive bonding has become a widely used joining method in engineering structures, especially for composite material components. Because of this wide use, research to advance knowledge of adhesively bonded structures was conducted at Purdue University. This is the first of three reports that resulted from that research.

The thickness of the adhesive layer is an important parameter determining the performance of bonded lap joints. Many researchers have investigated the thickness effect on the joint strength by using the mode I fracture test of the double cantilever beam (DCB) with the adhesive sandwiched between the two beams. There are two basic trends reported about the thickness effect on joint strength (or, more strictly, fracture toughness of the adhesive). Bascom, et al. [1 and 2], Kinloch and Shaw [3], Ikeda, et al. [4], and Lee, et al. [5], found through DCB experiments that the adhesive strength (toughness) increased as the adhesive thickness decreased when the bondline was thick. When the bondline thickness was very thin, the strength decreased

as the adhesive thickness decreased, as depicted in figure 1. Gardon [6] and Daghyani, et al. [7 and 8], also found that the strength of the specimens decreased as the adhesive thickness decreased below a certain value. However, for these cases, the failure was observed to locate at the adherend/adhesive interface.

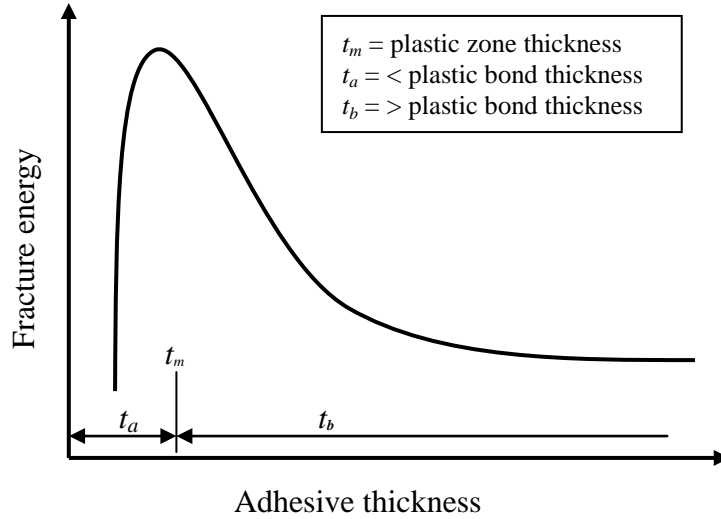


Figure 1. Adhesive Thickness Effect on Strength for Mode I Fracture

To explain the effect of adhesive thickness on the adhesive fracture toughness in their tapered double cantilever beam (TDCB) specimens, Kinloch and Show [3] proposed to use the confinement of the crack tip plastic zone to explain this effect. They noted that the fracture toughness is influenced by adhesive thickness and reaches the maximum value when the adhesive layer thickness is equal to the diameter of the plastic zone size (t_m , as shown in figure 2). At this adhesive thickness, they considered the plastic zone to be confined by the maximum degree of constraint, leading to the maximum volume of plastic deformation. When the adhesive layer thickness is lower than this value (t_a , as shown in figure 1), the plastic zone becomes smaller due to the constraint from the high-modulus adherends. The strength of the joint is lower for $t_a < t_m$. When $t_b > t_m$, the plastic zone is free from the constraint and the strength of the joint decreases to the value of bulk adhesive material. However, there was no experimental or numerical data presented in their paper. Further study is needed to verify this interpretation.

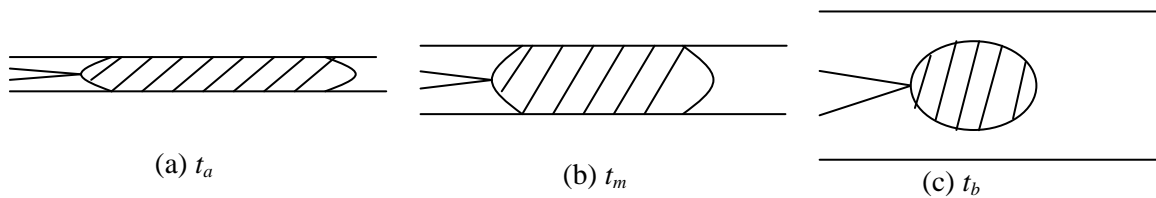


Figure 2. Traditional Explanation of Thickness Effect on Strength of Joints

The objective of the present study was to provide a rigorous fracture mechanics explanation for the adhesive thickness effect on the fracture strength of the DCB specimen. In addition, the crack tip opening angle (CTOA) was investigated as to its suitability to characterize the fracture toughness of highly confined adhesive in joints.

1.2 FRACTURE EXPERIMENT.

The DCB specimen shown in figure 3 was used to perform the fracture experiments. Two aluminum 7075 alloy panels with a thickness (t_a) of 3.175 mm and a width of 30 mm were used as the adherends. The adhesive used was Hysol[®] EA 9394[™], a popular aerospace-grade adhesive. A precrack was created by embedding a razorblade at the mid-plane of the adhesive layer before it was cured. Before the razorblade was inserted into the adhesive layer, it was coated with a mold release agent so the razorblade could be removed without causing damage to the adhesive material. The initial crack length (l) was 38 mm. The specimen was cured at room temperature for 12 hours followed by a 2-hour postcure at 150°F. After the adhesive was fully cured, the razorblade was removed from the adhesive layer leaving an initial crack of 38 mm long. Subsequently, these specimens were cut into two pieces using a water jet cutting machine. The final DCB specimen dimensions were 12.7 mm wide (W) and 100 mm long (L). Steel hinges were attached to the specimen to aid in the loading application. Nine adhesive thicknesses (t) were considered in this study: 0.4, 0.45, 0.7, 0.85, 0.95, 1.17, 1.3, 2.2, and 3.3 mm.

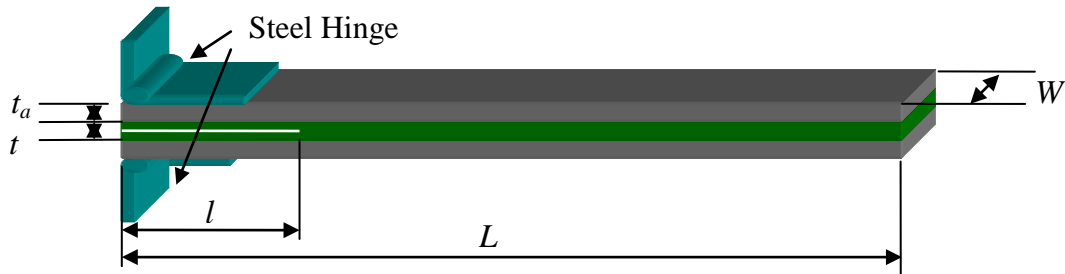


Figure 3. Specimen Configuration

The DCB specimens were loaded with a constant stroke rate of 0.01 mm/s at the opening end of the specimen using a 1-kip MTS testing machine. The load-displacement curves are shown in figure 4. The peak fracture loads of the specimens with different adhesive thicknesses are presented in figure 5. The relation between the fracture load and the adhesive layer thickness shows a similar trend as the curve shown in figure 1. When the adhesive layer is thick, the fracture strength increases as the bondline thickness decreases. After the strength of the specimen reaches the peak at an adhesive layer thickness of approximately 0.8 mm (t_m), the strength of the DCB specimen decreases as the adhesive layer decreases. For all specimens tested, there was adhesive residue on both sides of the failure surfaces. All the specimens appear to have failed in cohesive failure.

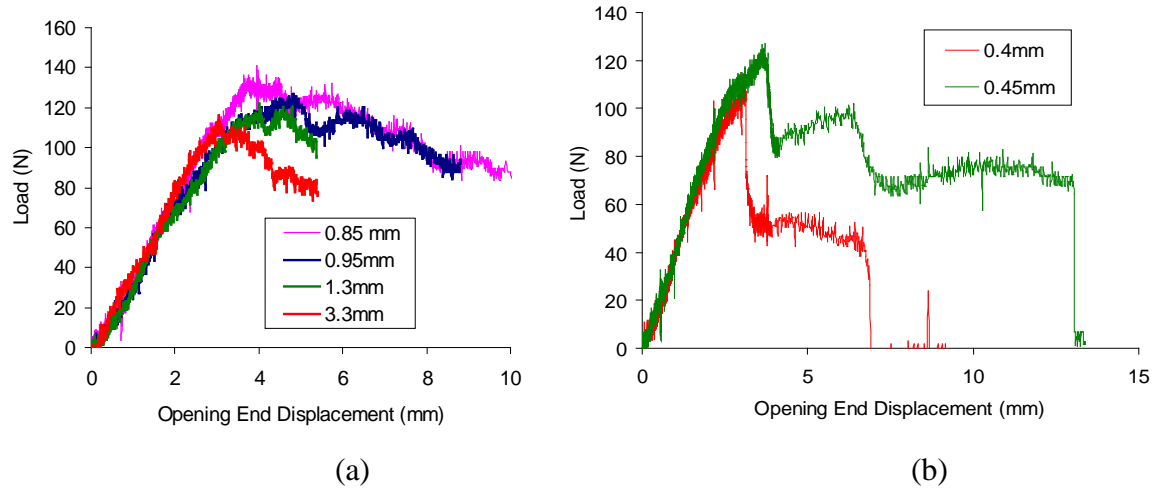


Figure 4. Load vs. Displacement Curves for Specimens With Different Adhesive Layer Thicknesses: (a) Thicker Specimens, Stable Load Decreases After Peak Load and (b) Thinner Specimens, Sudden Load Drop After Peak Load

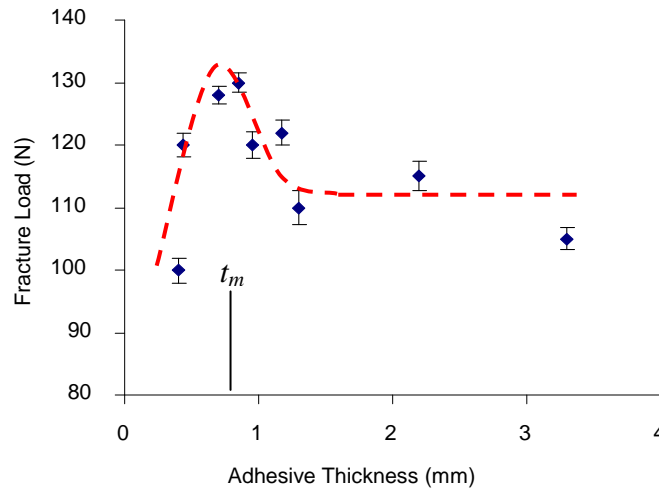


Figure 5. Experimental Results of Specimen Strength vs. Bondline Thickness

Elastic analyses of DCB specimens were performed using commercial code ABAQUS Version 6.6.1. Figure 6 shows the half model used in the analysis because of symmetry. The typical finite element analysis (FEA) mesh is shown in figure 7. The elastic moduli for aluminum are $E = 71.75$ GPa, Poisson's ratio $\nu = 0.33$, and for the Hysol EA 9394, $E = 4.33$ GPa and $\nu = 0.35$. Based on the failure load tested in the experiments, the critical energy release rates of DCB specimens with various bondline thicknesses were calculated by the modified crack closure method (with the results shown in figure 8), which indicates that the critical energy release rate (fracture toughness) is not a constant value but is dependent on bondline thickness. The question is why the fracture toughness is not a material constant.

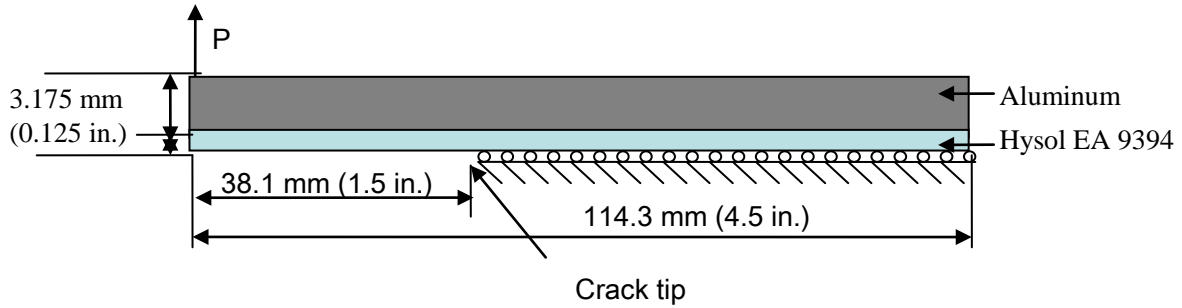


Figure 6. Configuration of the Finite Element Model

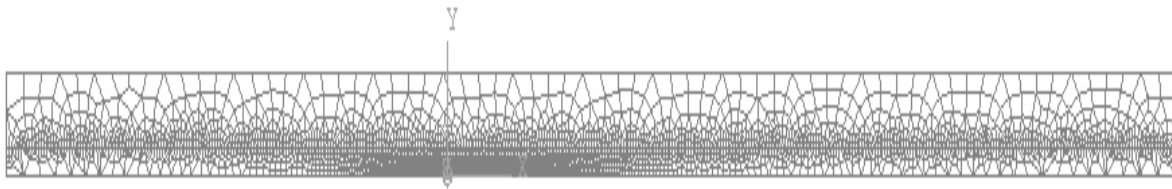


Figure 7. Typical FEA Mesh of DCB Specimens

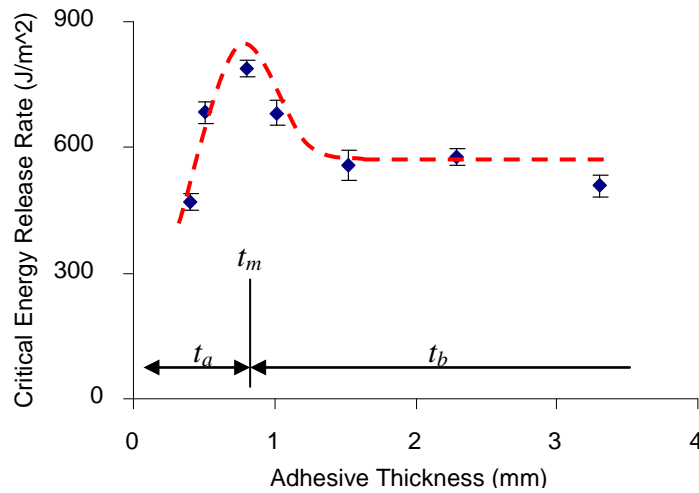


Figure 8. Energy Release Rate of DCB Specimens With Various Bondline Thicknesses

1.3 THE K-FIELD REPRESENTATION.

To use stress intensity factor or energy release rate to characterize fracture toughness of a material, the K-field (or the singular stress field represented by the stress intensity factor) must be the dominant stress in the fracture process zone [9]. For elastic-plastic materials, the K-field must be significantly greater than the plastic zone ahead of the crack tip. The total opening stress ahead of the crack tip can be expressed in a general form as

$$\sigma_{yy} = \frac{K}{\sqrt{2\pi x}} + \text{nonsingular stress} \quad (1)$$

where K is the stress intensity factor and x is the distance from the crack tip. At a given location, x , the weight of the singular term can be quantified by the degree of K-dominance defined as

$$\Lambda = \frac{\sigma_{yy}^{Singular}}{\sigma_{yy}^{Singular} + |\sigma_{yy}^{Nonsingular}|} \quad (2)$$

where

$$\sigma_{yy}^{Singular} = \frac{K}{\sqrt{2\pi x}}$$

$$\sigma_{yy}^{Nonsingular} = \sigma_{yy} - \sigma_{yy}^{Singular}$$

The value of Λ represents the singular stress percentage in the total opening stress at a given location.

Figure 9(a) shows the degree of singularity for the DCB models with four different adhesive layer thicknesses. The curves show that the degree of K-dominance falls below 90% in a very short distance (less than 0.1 mm) for all cases, as shown in figure 9(b). In other words, the singular stress term represented by K may not be sufficient to describe the failure force in the fracture process zone.

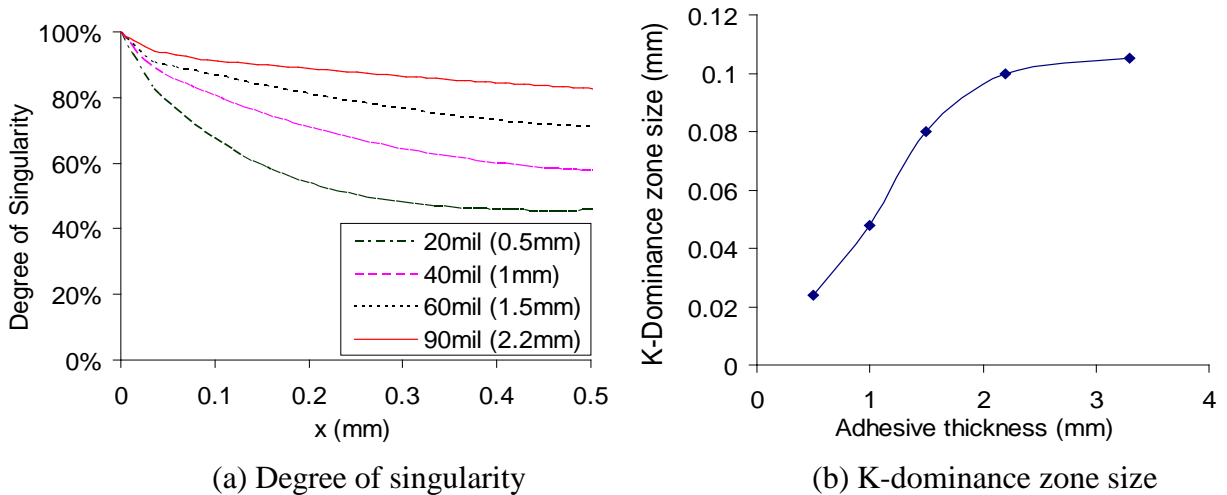


Figure 9. Degree of Singularity for DCB Specimens With Different Bondline Thicknesses

Another check is the K-dominance zone size relative to the plastic zone size at failure. If the plastic zone is not small compared to the K-dominance zone, then the small-scale yielding assumption is not valid, and linear elastic fracture mechanics is not adequate for characterizing fracture toughness.

A dog-bone-shaped specimen was used to measure the stress-strain curve for Hysol EA 9394. Because of the brittle nature of this material, the test specimen always failed around 1% strain. To perform an accurate elastic-plastic analysis, a curve that covers a wider range of strain was desired. Fortunately, a similar test of the same adhesive material was performed by Sandia National Laboratories [10] with a greater range, as shown in figure 10. The initial part of the Sandia curve coincides with the results of the dog-bone specimen test data. This curve was then extended (the dashed line) for the present elastic-plastic analysis.

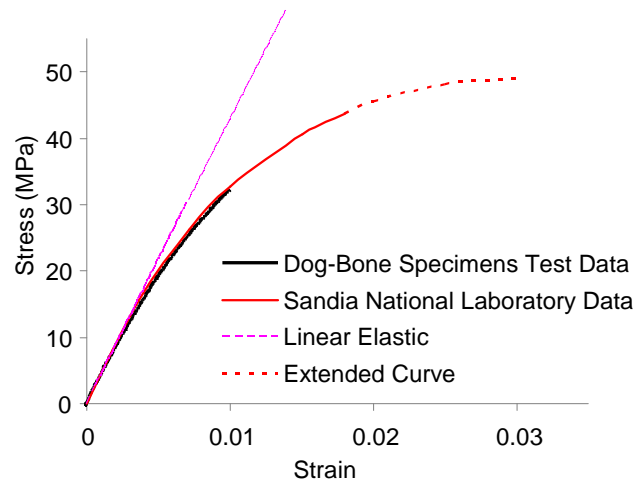


Figure 10. Stress-Strain Curve of Hysol EA 9394 Adhesive Material

Elastic-plastic analyses of DCB specimens were performed using commercial code ABAQUS Version 6.6.1. Due to the low-stress state in the aluminum adherends, the linear elastic material property was still applied for the aluminum in this elastic-plastic analysis. The four-node plane strain element (CPE4) was used for the entire model. Considering the high-stress concentration around the crack tip region, a very small (0.01-mm) mesh size was adopted.

Figure 11 shows two typical DCB specimens' plastic zones with two different bondline thicknesses subjected to the respective failure loads. Comparing to the K-dominance zone size presented in figure 9(b), the DCB specimens' plastic zones under the failure load is much larger than the K-dominance zone size for models with the same bondline thickness. This explains why the linear elastic fracture mechanics (LEFM) failed to predict the strength of the DCB specimens with different bondline thicknesses. Moreover, because of the plastic zone's large size under the failure load, the small-scale yielding assumption adopted in the LEFM was violated. Thus, an elastic-plastic analysis is needed to predict the DCB specimen's failure load.

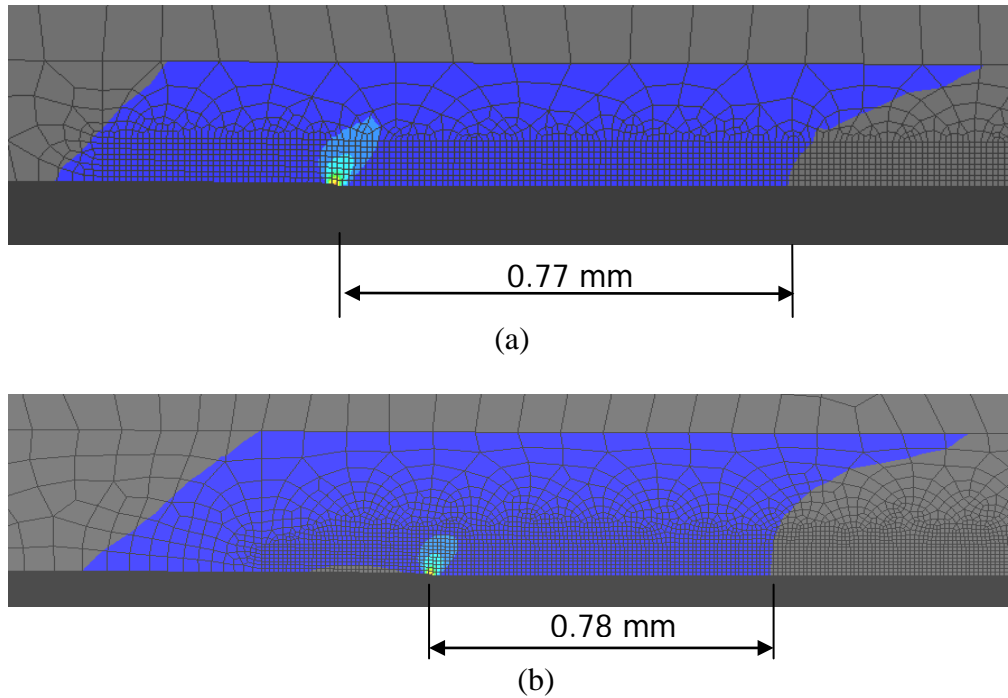


Figure 11. DCB Models' Plastic Zone Sizes Under Failure Load: (a) DCB Model With 0.4-mm Adhesive Thickness and (b) DCB Model With 0.8-mm Adhesive Thickness

1.4 THE CTOA AS A FRACTURE PARAMETER.

During the DCB specimen test, the load and opening-end displacement were tracked and recorded. The side view of the crack tip was also observed and recorded using a digital camera connected to a microscope. The initial crack created by the embedded razorblade in the adhesive layer is shown in figure 12(a). As the load increased, the opening angle of the crack also increased. Figure 12(b) shows the crack tip just before the onset of crack propagation. The entire crack opening and initiation process was recorded continuously. Because the difference between the initial angle and the onset of crack propagation is of interest, henceforth, this angle is referred to as CTOA. In this study, the CTOA was obtained by averaging the angles measured at four points of equal spacing located within the region of 0.2 mm behind the crack tip. Figure 13 shows how each angle is calculated based on the opening of the crack surfaces and the distance from the crack tip. Figure 14 shows the CTOA values from the elastic-plastic FEA corresponding to the failure loads of specimens with different adhesive thicknesses.

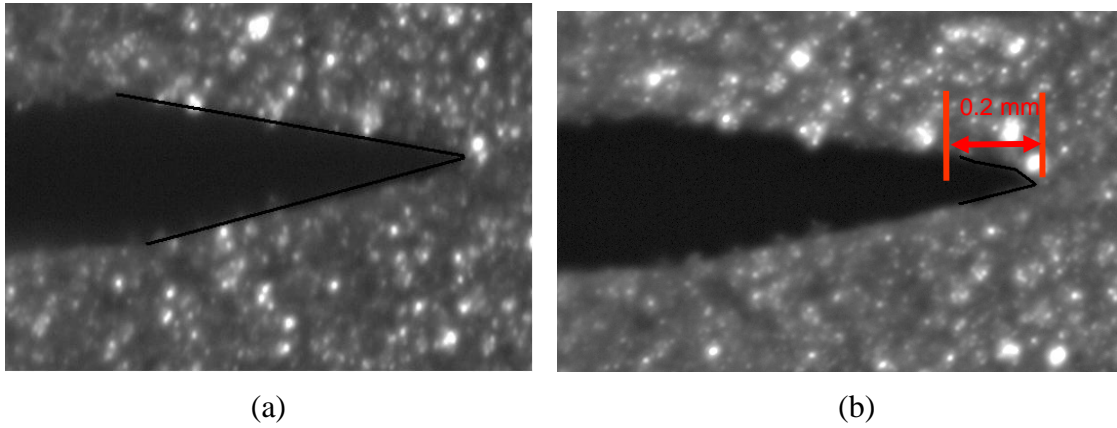


Figure 12. The Angle Change Before Crack Initiation: (a) Initial State and (b) Loaded

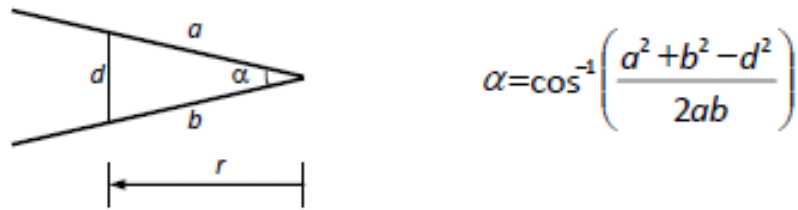


Figure 13. Calculation of CTOA

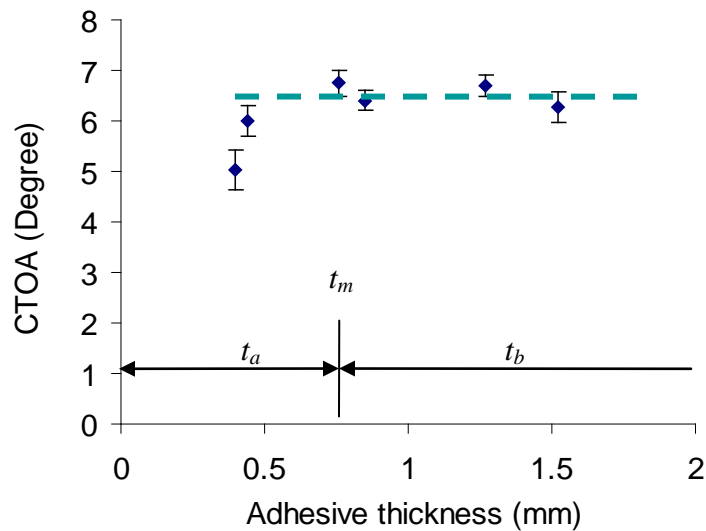


Figure 14. Crack Tip Opening Angle vs. Adhesive Thickness

As noted in figure 12, for specimens with an adhesive thickness greater than 0.8 mm (t_b region in figure 8), the CTOA values are more or less constant within the measurement scatter. In this region, it appears that a single constant CTOA value of 6.7° is able to characterize the fracture toughness of the adhesive independent of adhesive thickness. However, when the adhesive

thickness falls below 0.8 mm, the corresponding CTOA value decreases as the adhesive thickness decreases. This phenomenon correlates to the load-displacement curves presented in figure 4. Figure 4(a) shows four typical specimen curves with adhesive layer thicknesses greater than 0.8 mm. These curves exhibit a stable decrease in load after the peak load is reached. This is a normal stable crack growth behavior in a DCB specimen as the crack length increases after crack initiation. On the other hand, the two curves shown in figure 4(b), associated with the specimens containing adhesive layers thinner than 0.8 mm, show a sudden load drop after the peak load. This indicates that, instead of the expected mode I fracture, there may be a change in failure mode. An examination of the recorded image near the crack tip reveals that a new debonding crack along the adhesive/adherend interface is present in these specimens, see figure 15(b). The location of this interfacial failure lies about 0.3 mm from the crack tip. It should be noted that the debonding crack does not seem to be the result of adhesive failure, as a very thin layer of adhesive is left on the aluminum. For the specimens with thicker adhesive layers, the crack propagated in the adhesive, as shown in figure 15(a).

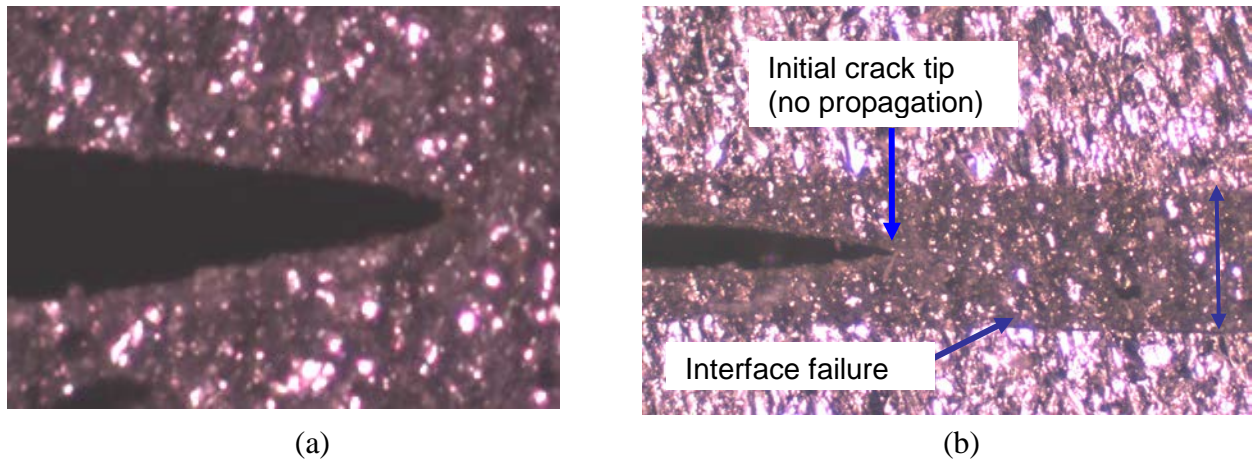
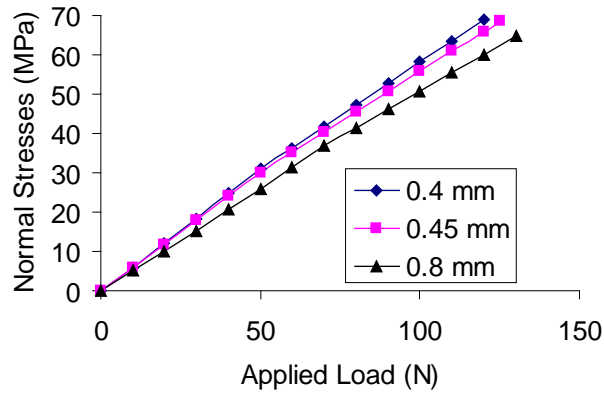
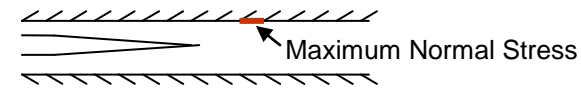


Figure 15. Crack Propagation for Specimens With Different Adhesive Layer Thicknesses
 (a) in Thicker Specimens, the Crack Initiated and Propagated Within the Adhesive Layer and
 (b) in Thinner Specimens, Interface Failure Occurred Before Crack Propagation

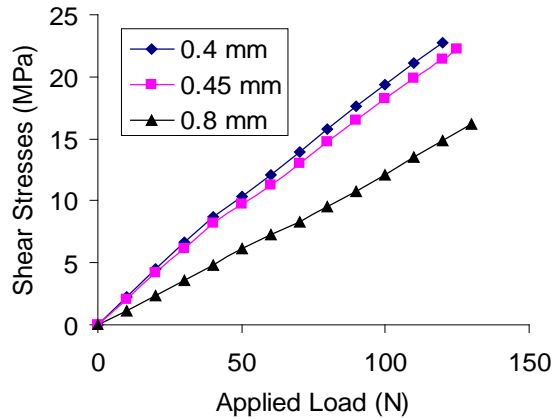
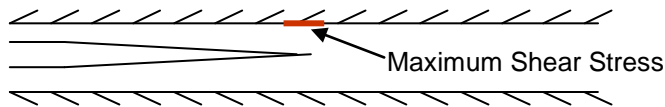
1.5 INTERFACIAL FAILURE.

The constant CTOA can be used as the fracture failure criterion to predict the strength of the DCB specimens under mode I fracture for adhesive thicknesses greater than 0.8 mm. When the adhesive thickness is less than 0.8 mm, the interface failure becomes the dominant failure mode, and CTOA is not adequate for the prediction of failure in DCB specimens. Thus, a closer look at the interfacial failure mechanism is needed.

Interfacial stresses between the aluminum beam and the Hysol adhesive are extracted from the FEA of three DCB models with different adhesive thicknesses (0.4, 0.45, and 0.8 mm). Figure 16(a) shows the maximum normal stress at the interface versus the applied load. It can be observed that, for the same applied load, the normal stress increases as the adhesive thickness decreases. Figure 16(b) shows the same trend for the maximum shear stress along the interface.



(a)



(b)

Figure 16. Maximum Stress Components Along the Interface vs. Load (Location and Value):
 (a) Maximum Normal Stress and (b) Maximum Shear Stress

Figure 17 shows the interfacial normal stress distributions under the respective failure loads for three adhesive thicknesses. It is interesting to note that the maximum normal stress occurs in the region of 0.25 to 0.3 mm from the crack tip. However, the maximum normal stress for the 0.8-mm adhesive layer is lower than the maximum normal stress for the 0.4- and 0.45-mm adhesive layers. Comparing the location of the maximum normal stress with the experimental result shown in figure 15(b), it is reasonable to conclude that the interfacial failure is caused by normal stress rather than shear stress. In fact, the location for the maximum shear stress occurs at the interface right above (and below) the crack tip.

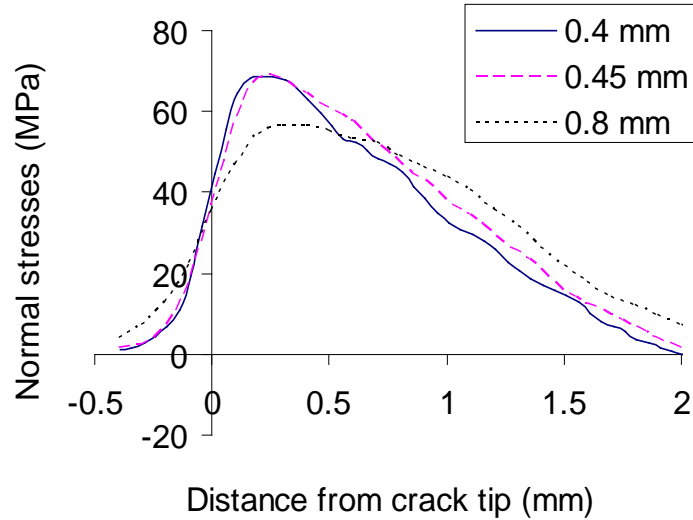


Figure 17. Normal Stress Distribution Along Interface Near Crack Tip

In the experiment, the two specimen groups with thinner adhesive layers (0.4 and 0.5 mm) failed with an interface failure, while the specimens with a 0.8-mm adhesive layer failed with mode I fracture. The similar maximum stresses from the models with thinner adhesive layers (0.4 and 0.5 mm) indicate that the specimens failed at a certain critical stress before the crack initiated from the original crack tip. For the specimens with an adhesive layer thicker than 0.8 mm, the mode I fracture failure was the dominant failure mode. The crack initiated from the original crack tip before the normal stress along the interface reached the critical value.

Both the interfacial normal and shear stresses increased quickly as the adhesive thickness decreased. When the adhesive is thick, the crack tip region reached the failure point first. The failure initiates from the original crack tip, and the original crack's initiation is controlled by the CTOA parameter. As the adhesive grows thinner, the interfacial stress becomes greater for the same loading. Until reaching a certain specific thickness, the interfacial stress reached the failure point before the original crack tip. Then, the interfacial crack appeared before the initiation of the original crack tip, causing the sudden loading drop during the continuous loading of the specimens. By then, the CTOA at the original crack tip would not yet have reached the critical value. Thus, the CTOA values measured in specimens with a very thin adhesive layer at the highest load point is smaller than the constant critical CTOA value.

In the FEA simulation, the CTOA value was calculated by applying experimental failure load on the models with very thin adhesive layers that were smaller than the constant critical CTOA value. Hence, for DCB specimens with a very thin adhesive layer, the constant CTOA criterion might overpredict the strength of the specimen. The interfacial stress analysis is necessary to the strength prediction.

1.6 CRACK TIP OPENING ANGLE—CRITERION AND ANALYSIS.

The results presented in section 1.5 indicate that a constant CTOA value can be used as a fracture criterion to predict the mode I fracture in adhesively bonded DCB specimens if the interface failure does not occur before crack extension. For Hysol EA 9394, this critical thickness was approximately 0.8 mm, and the CTOA was 6.7° .

As discussed in section 1.2, the initial crack in the DCB specimen was created by embedding the razorblade in the adhesive layer before curing. Consequently, the physical crack tip has a small but finite angle before loading. The CTOA is defined as the increased CTOA at the onset of fracture over the initial value. For a natural crack, the initial CTOA is nil, and the crack tip angle is the total angle. To determine whether this incremental angle can be used for natural cracks, a study was conducted on the effect of initial CTOA, before loading, on the validity of its application on natural cracks.

Figure 18 shows the finite element models for the natural crack tip and the crack tip created by a razorblade. The model shown in figure 18(b) is the actual shape of the initial crack tip adopted in the DCB specimen. For these two models, the actual failure loads are applied, and the CTOA values are calculated. Figure 19 shows the comparison of the CTOA values obtained from these two models under an applied load of 100 N. The difference between the two results is not significant. For practical purposes, a model with an ideal initial crack tip shape can be used to represent the crack in the actual specimens.

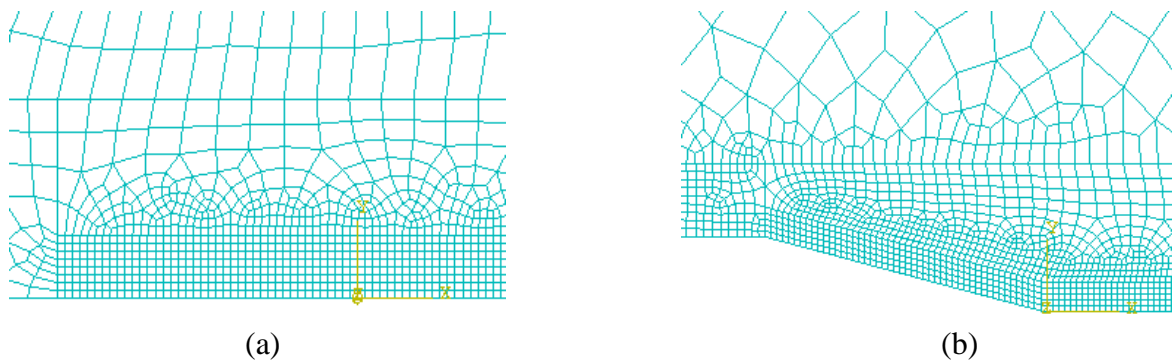


Figure 18. (a) Natural Initial Crack Configuration and (b) Crack Tip Created by the Razorblade

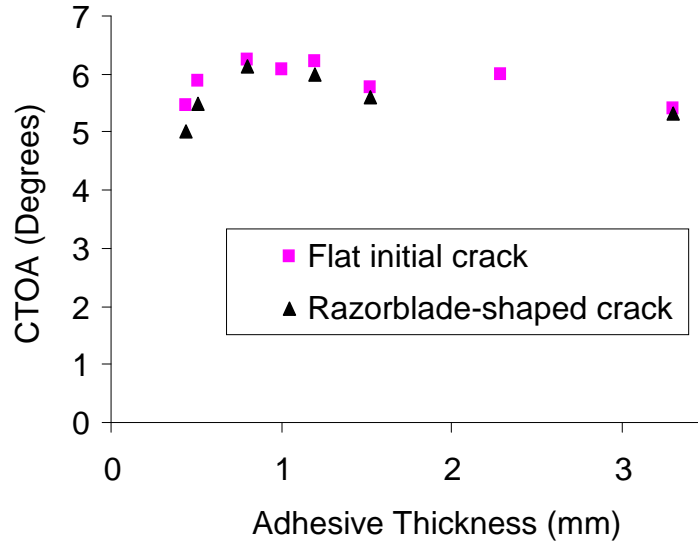


Figure 19. The CTOA Values at a Constant Applied Load From Models With Different Initial Crack Configurations

During the experiments, the load began to decrease once the crack initiated from the original razorblade crack tip. The highest DCB specimen's load was reached just before crack initiation, which is the critical point of the DCB specimens. Hence, models with experimental failure loads were also simulated to get the critical initial CTOA values. Figure 20 shows the initial CTOA values of DCB specimens (represented by purple diamonds) with different adhesive thicknesses under a corresponding failure load. The critical CTOA values are almost constant, except for the models with adhesive layers greater than 0.8 mm. When the adhesive thickness went below 0.8 mm, the CTOA value decreased as the thickness decreased. The experimental data and FEA simulations matched very well.

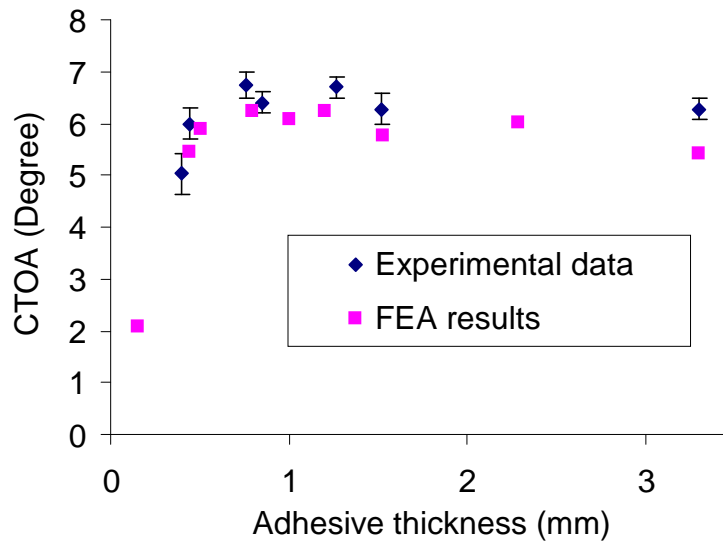


Figure 20. The CTOA Values Under Thickness-Dependent Failure Load

For the constant CTOA region (t_b , as shown in figure 20), the CTOA value is approximately 6.7° for both FEA simulation and experimental measurement. Figure 21 shows the failure loads for DCB specimens with various adhesive thicknesses predicted with a CTOA of 6.7° . It is shown that the failure load predicted by a constant CTOA matches the experimental data quite well until the adhesive thickness went below 0.8 mm. For the models with adhesive thickness less than 0.8 mm, the FEA prediction still increased as the adhesive thickness decreased, while the experimental data decreased. When the adhesive layer is thicker than 0.8 mm, the constant CTOA criterion very closely predicts the failure load of the DCB specimen. During the test, observations of the crack initiation showed that the DCB specimens experienced mode I fracture failure when the adhesive layer was thicker than 0.8 mm. Hence, it can be concluded that the constant critical CTOA criterion can be applied to the prediction of the failure strength of a DCB specimen if the failure is mode I fracture. The CTOA is a good representation of the elastic-plastic deformation of the crack tip at the onset of fracture and is independent of the adhesive thickness. When the adhesive layer is thinner than 0.8 mm, the failure loads of DCB specimens predicted by applying the constant CTOA criterion deviate greatly from the experimental data. It was observed experimentally that, in these specimens, an interfacial failure occurred ahead of the crack tip before the crack initiated from the original razorblade crack tip. The CTOA value measured at the onset of aluminum/adhesive interface failure was lower than the constant CTOA value for adhesive thicker than 0.8 mm. The adhesive material close to the interface failed before the original crack reached the failure point (constant critical CTOA value). This premature failure resulted in a different DCB strength trend with respect to adhesive thickness.

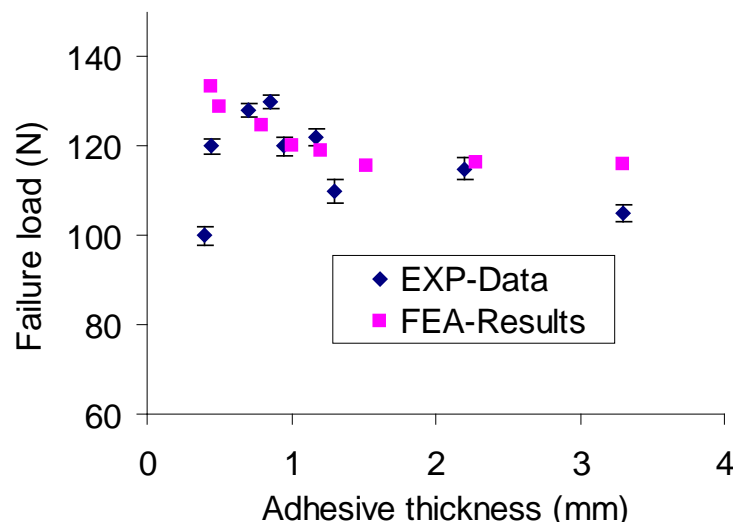


Figure 21. Mode I Fracture Strength Prediction Using the Constant CTOA Criterion

2. DEVELOPMENT OF FAIL-SAFE HYBRID JOINTS.

2.1 INTRODUCTION.

The hybrid joint technique has been studied by several researchers [11-19]. An analytical investigation was conducted by Hart-Smith [11] on a hybrid joint with stepped lap joints between titanium and carbon fiber-reinforced plastic adherends. The strength of the hybrid joints was the

same as well-designed bonded joints. In the peripheral of this problem, many researchers [12-15] proposed different numerical approaches and analytical solutions to analyze hybrid joints. Chan and Vedhgiri [13] conducted experiments with composite joints as well as a parametric study using finite element analysis to study the stacking sequence effect on joint strength. In that work, it was also observed that bolts do not take an active role in load transfer before the initiation of failure in bonding, which was also noted by Hart-Smith [11]. Barut and Madenci [14] developed a semi-analytical solution method for stress analysis of a hybrid joint, and observed that most of the load was transferred through the adhesive, even though it had lower modulus than the bolt. Kweon, et al. [17], observed a similar phenomenon in their experiments, where a double lap hybrid joint was considered using composite and aluminum adherends. The conventional hybrid joint is shown in figure 22.

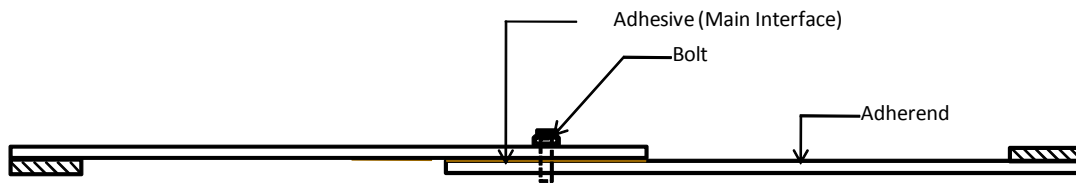


Figure 22. Conventional Hybrid (Bonded/Bolted) Joint

Matsuzaki, et al. [18], used a different approach to prepare a hybrid joint, using a bolted/co-cured technique, to avoid drilling holes in the fabricated composite parts. The resulting single lap hybrid joints of glass fiber-reinforced plastic and aluminum were tested with an expectation that the hybrid joint would have a higher strength compared to the co-cured (bonded) joint. The improvement in the hybrid joint strength was rather insignificant. In the force-displacement curve of the hybrid joint, there are two segments: one corresponds very closely to the bonded joint and the other to the bolted joint. Therefore, even manufacturing techniques cannot improve the performance of a hybrid joint over a bonded joint, except for achieving fail-safe design due to the presence of bolts.

In all existing hybrid joint designs, bolts do not carry loads until almost after the complete failure of the bondline. In other words, bolts stay idle until the failure in the bonded part of the joint occurs. It is evident that to improve the hybrid joint, a new design is needed in which the bolts would contribute to the load bearing at the joint before the complete failure of the adhesive.

Other forms of improving adhesively bonded joints have been pursued. Qian and Sun [20] proposed an idea of using attachments to provide additional load transfer paths at a double-strap joint. Along with additional load transfer paths, this proposed design reduces the localized interfacial stress concentrations near the joint edges. The strength of the joint with attachments was 20%-30% greater than the conventional double-strap joint. A similar approach was employed by Turaga and Sun [21] to improve single lap bonded joints. In reference 21, experiments were conducted with aluminum as well as composite adherends. Failure loads for conventional single lap joints and single lap joints with attachments were compared. There was a 59% increase in the bonded joint strength when using attachments. Recently, Kumar, et al. [22], proposed a new hybrid (bonded/bolted) joint with angular attachments. All the experiments in

reference 22 were conducted on joints with metallic adherends, aluminum alloy 2024-T3. The increase in joint strength of the new hybrid joint with attachments was approximately 80% higher compared to the conventional hybrid joint. The hybrid joint with angular attachments is shown in figure 23.

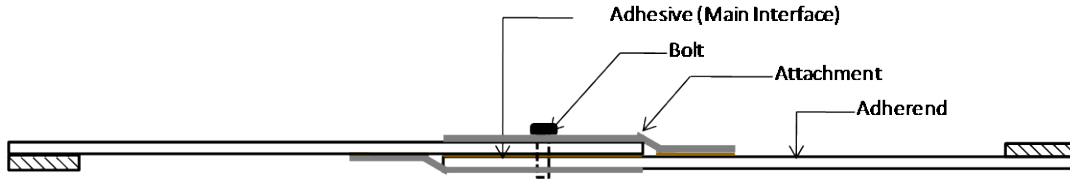


Figure 23. Hybrid Joint With Angular Attachments

In this study, a new hybrid joint design for composites was proposed. Instead of angular attachments, straight composite laminate attachments were used. In the proposed hybrid joint design, the bolt contributes to load transfer as soon as the joint is loaded.

2.2 EXPERIMENTS.

Experiments were conducted on five different joint configurations: bonded joint, bolted joint, conventional hybrid joint, and hybrid joint with attachments. The hybrid joint with attachments had two types, L-shaped and stepped.

AS4/3501-6 carbon/epoxy prepreg tape was used to fabricate a 20-ply laminate with a stacking sequence of $[0_2/90_2/0_3/90_2/0]_s$. The stacked laminates were cured in an autoclave, and a water jet cutting machine was used to obtain the desired dimensions of the adherends. The width of the specimens was kept at 38 mm. The same adherend thickness was maintained for all joint configurations. For the new hybrid joint with attachments, two types were prepared, L-shaped and stepped.

L-shaped attachments were composed of two flat composite laminate pieces (figure 24). The long flat piece was prepared with AS4/3501-6 prepreg tape, with a stacking sequence of $[0_2/90_2/0]_s$, which was half the total thickness of the adherend. The smaller piece was cut from the same panel for the adherends. These two flat attachment pieces were bonded together using Hysol EA 9394 structural paste adhesive.

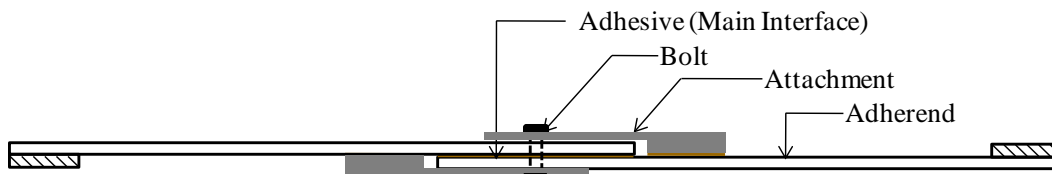


Figure 24. New Hybrid Joint With L-Shaped Attachments

To prepare the stepped attachments, four 0° AS4/3501-6 plies were stacked together and cured in an autoclave. Rectangular 25- x 38-mm pieces were cut using a water jet cutting machine. Four of the rectangular pieces were glued together in a stepped fashion. The top part of the stepped attachment was attached to the top flat attachment in the same manner as the L-shaped attachment.

For the final joint preparation, the adherends were bonded together with Hysol EA 9394 first, then the attachment was bonded to the adherends, as shown in figure 24. Subsequently, a diamond drill bit was used to drill a hole at the center of the overlapped region of the joint, and a titanium bolt was put in place and fastened. The last step was attaching tabs to the adherends to minimize load eccentricity in the single lap joint.

The final joint configurations are shown in figure 25. A magnified view of the hybrid joint with attachments, L-shaped and stepped, is shown in figure 26.

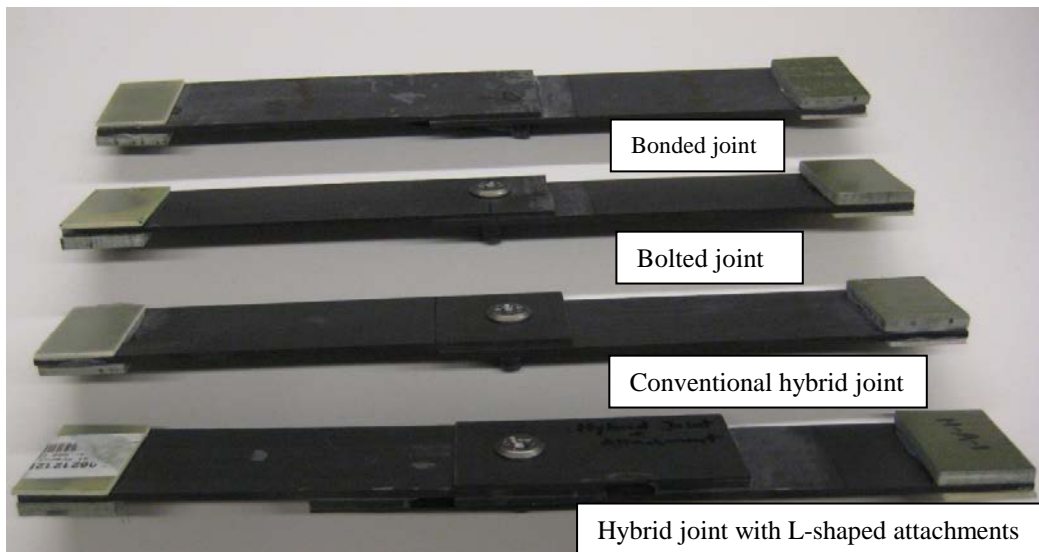


Figure 25. Final Joint Configurations

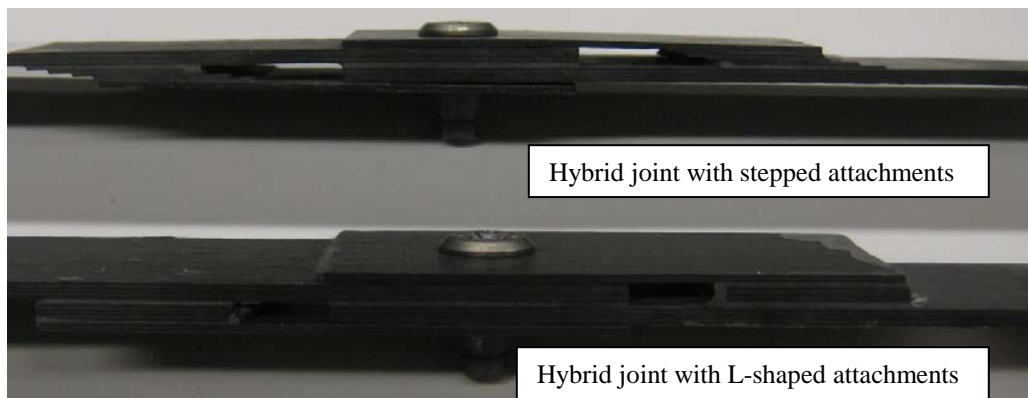


Figure 26. Magnified View of the L-Shaped and Stepped Attachments

2.3 RESULTS AND DISCUSSION.

All the following experiments were conducted on an MTS 22-kip machine at a crosshead displacement rate of 0.01 mm/sec.

2.3.1 Bonded and Bolted Joint.

Typical load-displacement curves for the bonded and bolted joints are shown in figures 27 and figure 28, respectively.

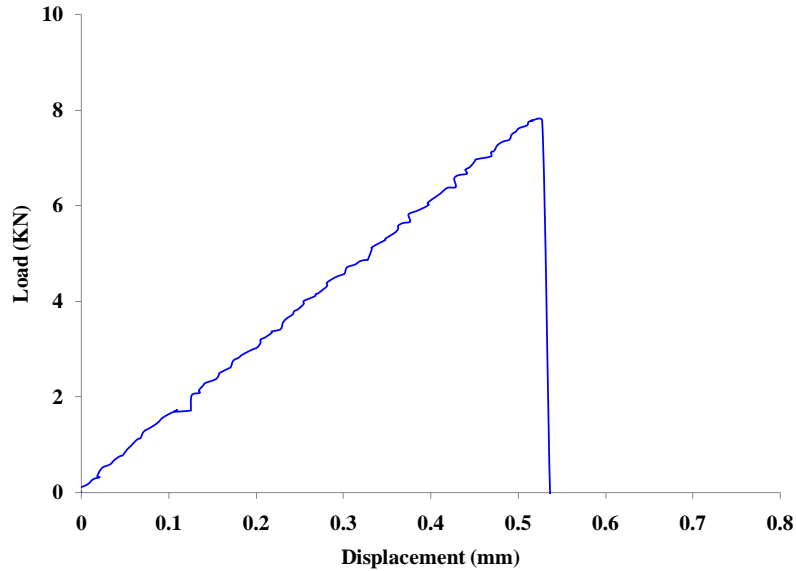


Figure 27. Load-Displacement Curve for the Composite Bonded Joint

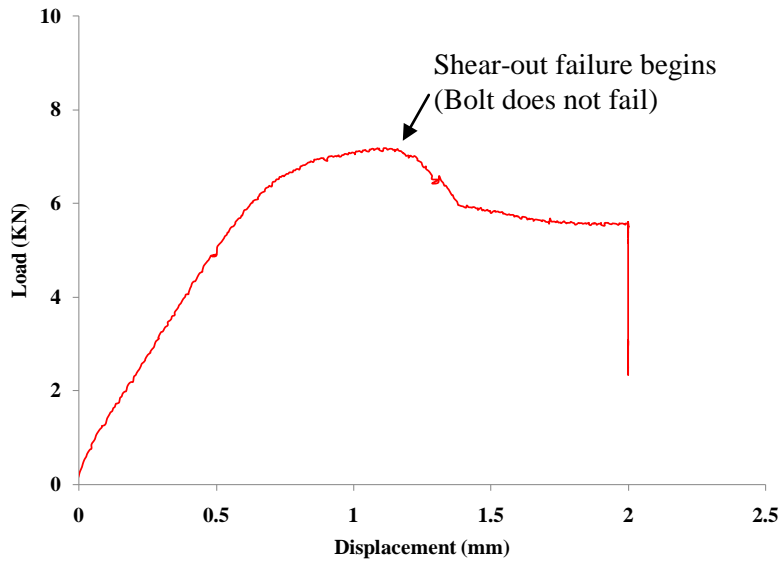


Figure 28. Load-Displacement Curve for the Composite Bolted Joint

The failure of the bonded joint was catastrophic and was similar to the metallic adherends in reference 22. The load-displacement curve varies linearly before failure. The failure load for the bonded joint was 8.5 kN. For the bolted joint, the peak load was observed a 7.3 kN. At this load, shear-out initiated in the composite adherends. As shear-out progressed, the adherends became weaker and the load decreased, as shown in figure 28. A typical failure around the bolthole location is shown in figure 29. The 0/90 degree laminates that were tested caused a shear-out failure instead of a bearing failure. Thus, the data shown here may not reflect the behavior of joints in actual practice.

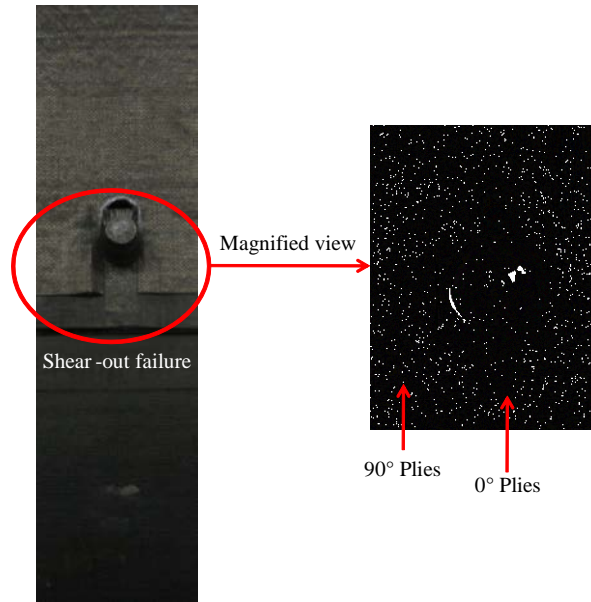


Figure 29. A Typical Shear-Out Failure Pattern Around the Bolt

2.3.2 Conventional Hybrid Joint.

A typical load-displacement curve is shown in figure 30. In this case, the failure process involved two steps. The first failure occurred as a complete debonding, similar to the bonded joint followed by the failure similar to the bolted joint. The first failure of the conventional hybrid joint occurred at a load slightly higher than the failure load of the bonded joint. The average initial failure load of the hybrid joint was 11 kN.

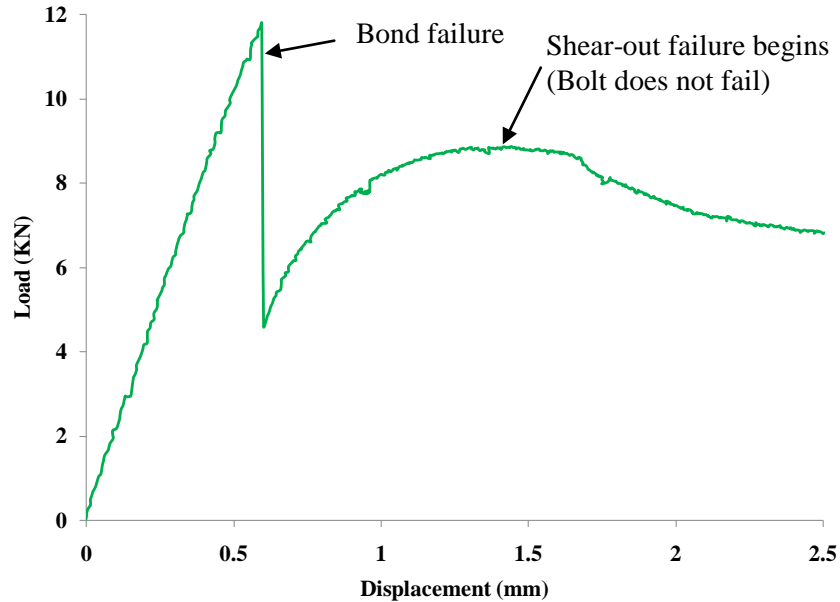


Figure 30. Load-Displacement Curve for the Conventional Hybrid Joint

2.3.3 New Hybrid Joint With Attachments.

Three specimens of each attachment type, L-shaped or stepped, were tested. The characteristics of the typical load-displacement curve were similar to that of the conventional hybrid joint, except for the level of the failure load.

2.3.3.1 Hybrid Joint With L-Shaped Attachment.

For the hybrid joint with L-shaped attachments, the first failure occurred at the main interface between the adherends and at the interface between the bottom part of the attachment and the adherend. After this failure, only the bolt carried the applied load. The load-displacement behavior is shown in the second segment of the curve in figure 31. The average strength of this joint configuration was 19 kN, which is around 75% more than the conventional hybrid joint.

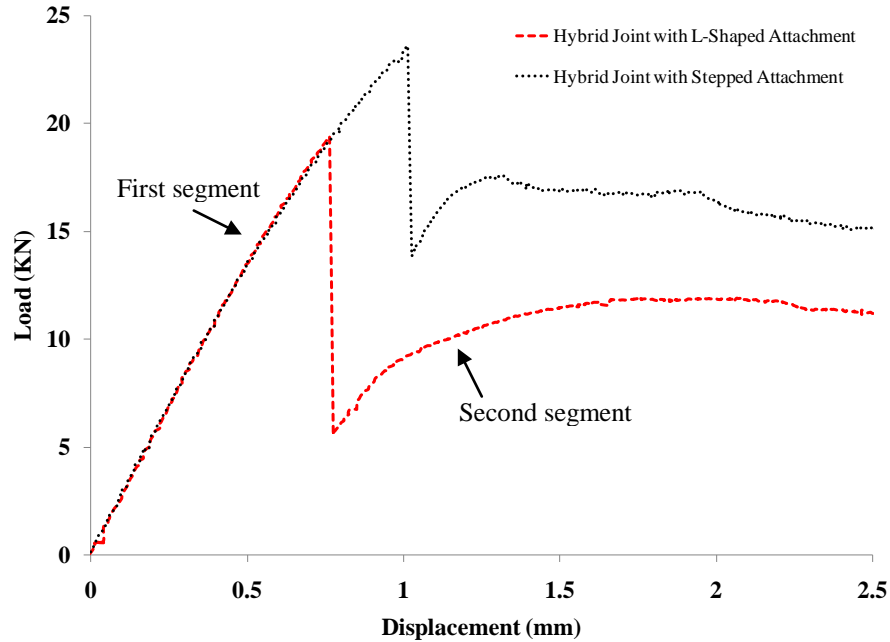


Figure 31. Load-Displacement Curves for Hybrid Joint With Attachments

2.3.3.2 Hybrid Joint With Stepped Attachment.

For the hybrid joint with stepped attachments, the load-displacement curve is shown in figure 31. The first failure occurred at the main interface between the adherends, whereas the stepped attachments remained bonded to the adherend. As the load increased, shear-out started in the same manner as the bolted joint case. This implies that the stepped attachment performed better than the L-shaped attachment. The average failure load for this joint configuration was 23.5 kN, which is 115% more than the conventional hybrid joint.

2.3.4 Comparison of All Joint Configurations.

For comparison purposes, the load-displacement curves for the bonded joint, the conventional hybrid joint, and the new hybrid joints are shown together in figure 32. It is clear that the hybrid joint with stepped attachments yields the best strength of these joint configurations. Figure 33 presents the strengths in a bar chart. The failure load for the hybrid joint with stepped attachment is 160%, 120%, and 20% higher than the bonded joint, the conventional hybrid joint, and the new hybrid joint with L-shaped attachments, respectively.

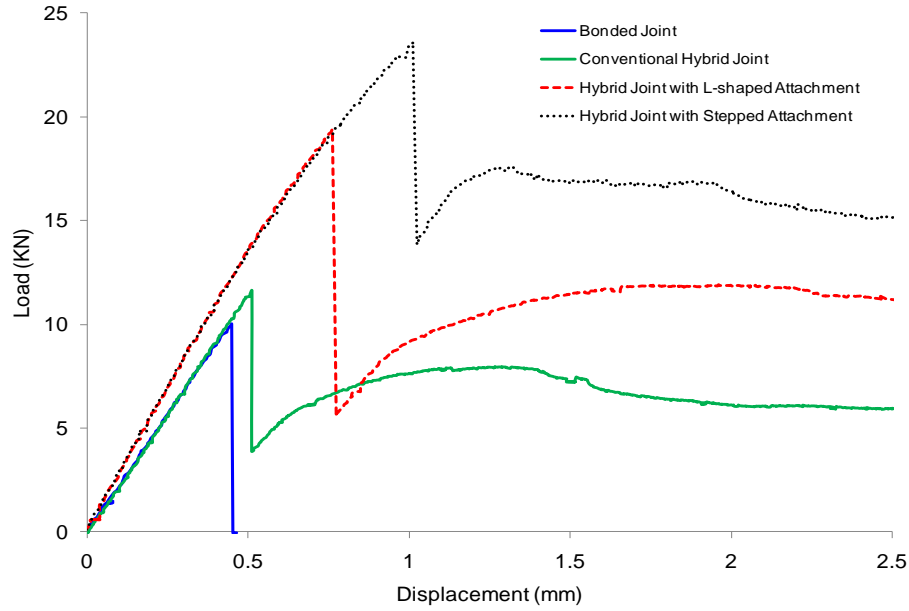


Figure 32. Load-Displacement Curves for All Joints

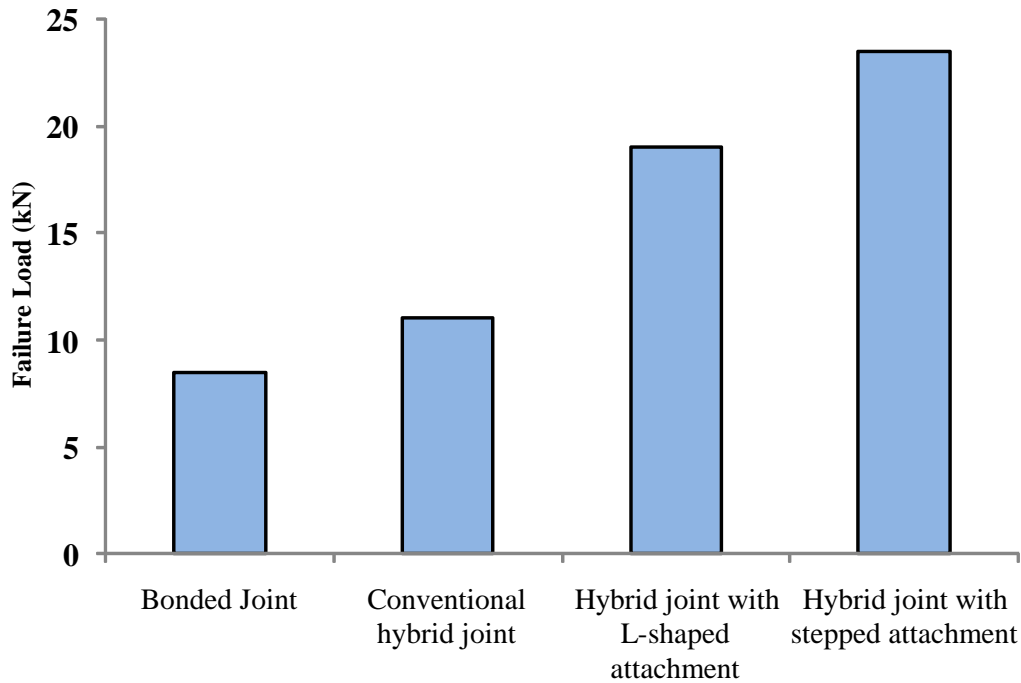


Figure 33. Comparison of Failure Loads for All Joint Configurations

2.3.5 Finite Element Analysis.

Plane strain FEA was performed using commercial code ABAQUS Version 6.8-1 to determine the effect of attachments on the hybrid joint. Since the initial failure of all hybrid joint types is due to debonding, a two-dimensional FEA should give a reasonable estimation of the effect of

attachments. Three cases were analyzed: bonded joints, hybrid joints with L-shaped attachments, and hybrid joints with stepped attachments. A typical stress pattern for all three configurations is shown in the figure 34.

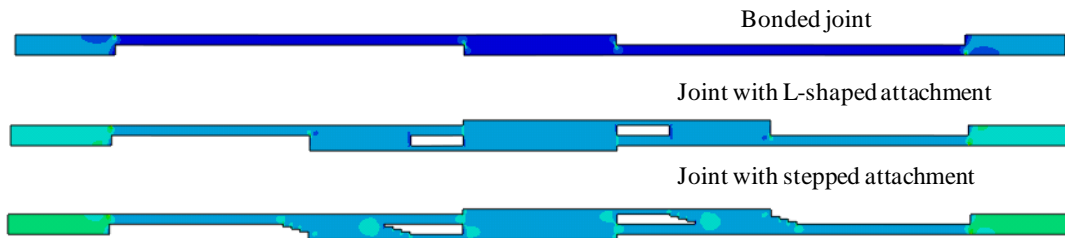


Figure 34. A Typical Stress Pattern for Three Joint Configurations

2.3.6 Peel Stress Distribution.

The peel stress distributions along the main interface of the three joint configurations are shown in figure 35. The peel stress distributions are calculated for the same applied load. It can be observed that the bonded joint has a higher peel stress compared to the other two hybrid joints with attachments. The peel stress variations along the length of the main interface of the hybrid joints with L-shaped and stepped attachments are very similar but are significantly lower than the peel stress of the bonded joint. This explains why the hybrid joints with attachments are stronger than the bonded joint.

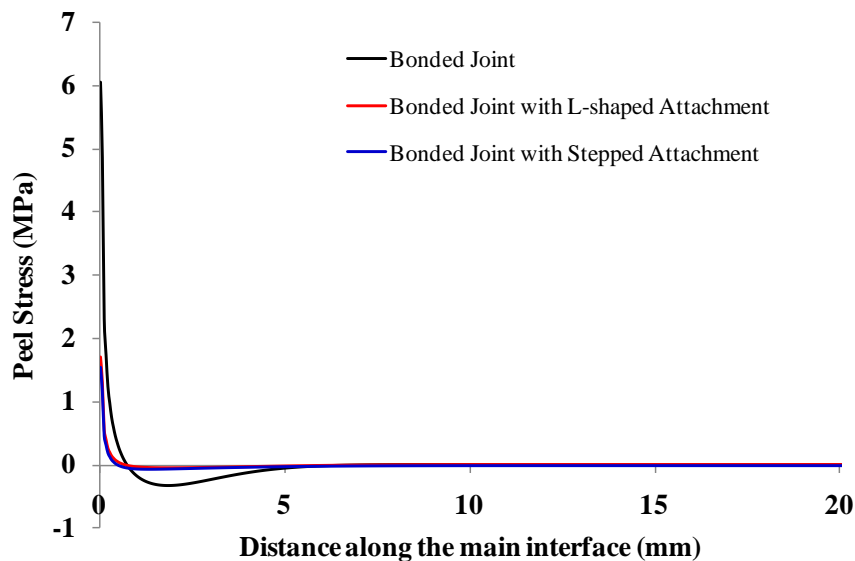


Figure 35. Peel Stress Distribution Along the Main Interface

Peel stress distributions along the interface between the adherend and the attachment of the hybrid joints with attachments are shown in figure 36. As shown in the figure, the peel stress at the end of the L-shaped attachment is greater than that of the stepped attachment. This explains why the hybrid joint with L-shaped attachments is lower than the hybrid joint with stepped attachments. Note that the peel stress is oscillatory due to the stepping of the attachment.

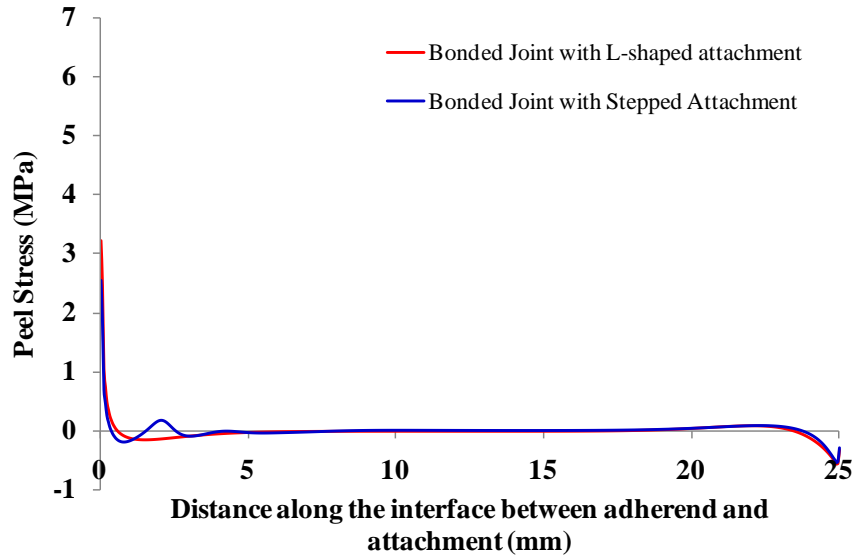


Figure 36. Peel Stress Distribution Along the Interface of the Attachment and the Adherend

2.3.7 Load Distribution.

For the hybrid joint with L-shaped attachments, load transfer distributions were calculated. It was found that 22% of the applied load was transferred to the attachment and the remaining 78% was transferred to the other adherend through the main interface (see figure 37). The optimization of the attachment shape can be done to transfer more loads through the attachment, thereby reducing the load on the main interface.

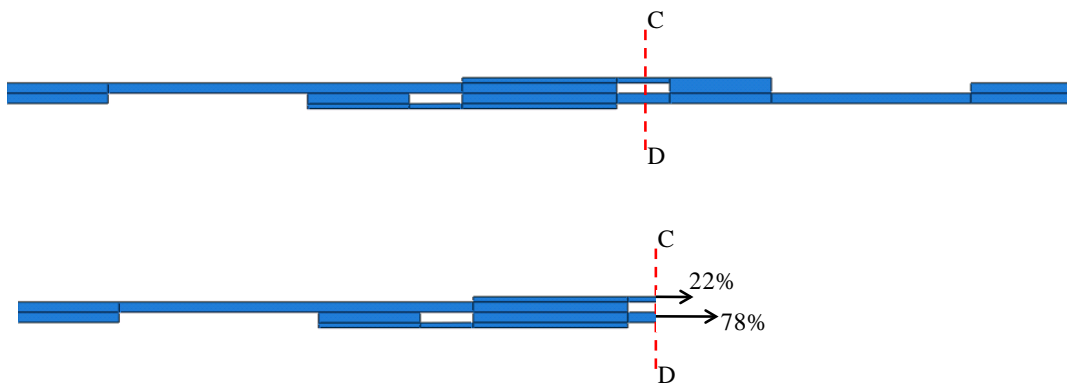


Figure 37. Load Distribution in the Hybrid Joint With L-Shaped Attachment

3. CONCLUSIONS.

3.1 EFFECTS OF BONDLINE THICKNESS CONCLUSIONS.

The value of the crack tip opening angle (CTOA) is not influenced appreciably by the adhesive thickness when the failure mode remains mode I fracture. Consequently, the adhesive thickness effect on the strength of double cantilever beam (DCB) specimens can be accounted for by using a constant CTOA as the fracture criterion. For specimens with very thin adhesive thicknesses, the dominant failure mode is shifted to the interface between the aluminum and the adhesive and failure is controlled by the interfacial normal stress, which is significantly influenced by the adhesive thickness. The geometry (e.g., created by the embedded razorblade) of the precrack tip has little effect on the CTOA value of the DCB specimens. The model with an ideally flat precrack is adequate for calculating CTOAs.

In general, the DCB specimen is not very suitable for testing mode I fracture toughness of adhesive materials because of exceedingly small K-dominance zone sizes it can produce, making stress intensity factor or energy release rate unsuitable for representing the driving force in the fracture-processing zone at the crack tip. The fracture strength of DCB specimens increased as the adhesive thickness decreased. In this range, the crack would propagate inside the adhesive layer. However, when the adhesive thickness dropped below 0.8 mm for Hysol EA 9394, the interfacial (adhesion) failure mode occurred before crack extension, and the strength of the DCB specimen starts to decrease with the decreased adhesive thickness.

3.2 HYBRID JOINT DESIGN CONCLUSIONS.

Five composite single lap joint configurations were tested. Bondline thicknesses were kept the same for all cases, wherever bonding was needed. A hybrid joint with attachments performed better than any conventional joint configurations, i.e., bonded or hybrid joints. Hybrid joints with stepped attachments performed better than hybrid joints with L-shaped attachments. The enhancements in the joint strength were 75% and 115% for the L-shaped and stepped attachments, respectively, over the conventional hybrid joint. Finite element analysis results indicate that the hybrid joint with stepped attachments experiences the lowest peel stress of the joint configurations considered. The 0/90 degree laminates that were tested caused the failure to be shear-out instead of bearing. Thus, the data shown here may not reflect the behavior of joints in actual practice.

4. REFERENCES.

1. Siegmund, T., "Adhesively Bonded Joints, Part 2: The Cohesive Zone Model for Analysis of Fracture and Damage Tolerance of Adhesively Bonded Joints," FAA report DOT/FAA/AR-11/1,P2, February 2014.
2. Hyonny, K., "Adhesively Bonded Joints, Part 3: Effect of Bondline Thickness on Mixed Mode Fracture of Adhesively Bonded Joints," FAA report DOT/FAA/AR-11/1,P3, February 2014.

3. Bascom, W.D., Cottington, R.L., Jones, R.L., and Peyser, P., "The Fracture of Epoxy and Elastomer-Modified Epoxy Polymers in Bulk and as Adhesives," *Journal of Applied Polymer Science*, Vol. 19, 1975, pp. 2545-2562.
4. Bascom, W.D. and Cottington, R.L., "Effect of Temperature on the Adhesive Fracture Behavior of Elastomer-Epoxy Resin," *Journal of Adhesion*, Vol. 7, 1976, pp. 333-346.
5. Kinloch, A.J. and Shaw, S.J., "The Fracture Resistance of a Toughened Epoxy Adhesive," *Journal of Adhesion*, Vol. 12, 1981, pp. 59-77.
6. Ikeda, T., Yamashita, A., Lee, D., and Miyazaki, N., "Failure of a Ductile Adhesive Layer Constrained by Hard Adherends," *Transactions of the ASME, Journal of Engineering Materials and Technology*, Vol. 122, 2000, pp. 80-85.
7. Lee, D.B., Ikeda, T., and Choi, N., "Fracture Behavior Around a Crack Tip in Rubber-Modified Epoxy Adhesive Joint With Various Bond Thicknesses," *Journal of Material Science Letters*, Vol. 22, 2000, pp. 229-233.
8. Gardon, J.L., "Peel Adhesion, I, Some Phenomenological Aspects of the Test," *Journal of Applied Polymer Science*, Vol. 7, 1963, pp. 625-641.
9. Daghyani, H.R., Ye, L., and Mai, Y.W., "Mode I Fracture Behavior of Adhesive Joints, Part I, Relationship Between Fracture Energy and Bond Thickness," *Journal of Adhesion*, Vol. 53, 1995, pp. 149-162.
10. Daghyani, H.R., Ye, L., and Mai, Y.W., "Mode I Fracture Behavior of Adhesive Joints, Part II, Stress Analysis and Constraint Parameters," *Journal of Adhesion*, Vol. 53, 1995, pp. 163-172.
11. Rybicki, E.F. and Kanninen, M.F., "A Finite Element Calculation of Stress Intensity Factors by a Modified Crack Closure Integral," *Engineering Fracture Mechanics*, Vol. 9, 1977, pp. 931-93.
12. Guess, T.R., Reedy, E.D., and Stavig, M.E., "Mechanical Properties of Hysol EA 9394 Structural Adhesive," Sandia National Laboratories, 1995.
13. Hart-Smith, L.J., "Bonded-Bolted Composite Joints," *Journal of Aircraft*, Vol. 22, 1985, pp. 993-1000.
14. Kelly, G., "Load Transfer in Hybrid (Bonded/Bolted) Composite Single Lap Joints," *Composite Structures*, Vol. 69, 2005, pp. 35-43.
15. Chan W.S. and Vedhagiri, S., "Analysis of Composite Bonded/Bolted Joints Used in Repairing," *Journal of Composite Materials*, Vol. 35, 2001, pp. 1045-1061.

16. Barut, A. and Madenci, E., "Analysis of Bolted-Bonded Composite Single Lap Joints Under Combined In-Plane and Transverse Loading," *Composite Structures*, Vol. 88, 2008, pp. 579-594.
17. Paroissien, E., Sartor, M., Huet, J., and Lachaud, F., "Analytical Two-Dimensional Model of a Hybrid (Bolted/Bonded) Single Lap Joint," *Journal of Aircraft*, Vol. 44, 2007, pp. 573-582.
18. Stewart, M.L., "An Experimental Investigation of Composite Bonded and/or Bolted Repairs Using Single Lap Joint Designs," *AIAA-97-1339: 2752-2760*.
19. Kweon, J., Jung, J., Kim, T., Chai, J., and Kim, D., "Failure of Carbon Composite-to-Aluminum Joints With Combined Mechanical Fastening and Adhesive Bonding," *Composite Structures*, Vol. 75, 2006, pp. 192-198.
20. Matsuzaki, R., Shibata, M., and Todoroki, A., "Improving Performance of GFRP/Aluminum Single Lap Joints Using Bolted/Co-Cured Hybrid Method," *Composites Part A*, Vol. 39, 2007, pp. 154-163.
21. Matsuzaki, R., Shibata, M., and Todoroki, A., "Reinforcing an Aluminum/GFRP Co-Cured Single Lap Joint Using Inter-Adherend Fiber," *Composites Part A*, Vol. 39, 2008, pp. 786-795.
22. Qian, H. and Sun, C.T., "Performance of a Composite Double Strap Joint With Attachments," *Joining and Repair of Composite Structures*, ASTM STP 1455, 2004.